AIMS Energy, 12(4): 905–923.
DOI: 10.3934/energy.2024042
Received: 05 February 2024
Revised: 18 June 2024
Accepted: 29 July 2024
Published: 06 August 2024

https://www.aimspress.com/journal/energy

Research article

Circuit simulation-based comparison of power electronics devices in a five-level converter for UAV applications

Enrico Alfredo Bottaro, Cristina Ventura and Santi Agatino Rizzo*

Department of Electrical Electronic and Computer Engineering, University of Catania, 95125 Catania

* **Correspondence:** Email: santi.rizzo@unict.it; Tel: +390957382308.

Abstract: In this paper, the performance of a 5-level cascaded H-bridge inverter in unmanned aerial vehicle (UAV) applications is analized to identify, at the converter design stage, the better device choice depending on different UAV operation scenarios. Considering that regardless of the specific application there are some typical operations, such as take-off, climb, land, cruise, and potential recurring climbs and descents, the results can support the choice by considering the typical working conditions of the specific application where the UAV would be used. The results have been obtained by simulating the H-bridge inverter considering the circuit models of insulated-gate bipolar transistors (IGBTs), GaN high-electron-mobility transistors (HEMTs), and Si and SiC metal-oxide-semiconductor field-effect transistors (MOSFETs) provided by manufacturers. The study has highlighted that the choice of the device depends on the UAV usage, switching frequency, and load conditions. More specifically, considering the typical devices and systems costs in the case of a selective harmonic elimination procedure operating at the fundamental switching frequency, the Si devices should be used. Moreover, the preference for using IGBTs or Si MOSFETs depends on the typical working conditions of the UAV application. In the case of phase-shift carrier modulation technique, at 4 kHz the MOSFET is the best device and the choice between Si and SiC devices depends on the UAV application's main operation scenarios. At 20 kHz the SiC MOSFET is the best device, while at higher frequencies the GaN HEMT cost should be faced to take advantage of its best performance.

Keywords: multilevel inverter; unmanned aerial vehicles; power electronics device; circuit model; circuit simulation

1. Introduction

Gallium nitride (GaN) and silicon carbide (SiC) wide bandgap semiconductors have a large atomic bond strength which provides high saturated electron speed and large breakdown field strength, and they show favorable characteristics including low conduction resistance, threshold voltage, capacitance, reverse recovery charge, etc. [1–3]. Thanks to these characteristics, GaN and SiC power devices will be used for high power density and high efficiency and will replace conventional silicon counterparts in applications ranging from 600 to 1700 V [4,5]. In terms of voltage rating, the drain-to-source voltage of GaN power devices is typically below 650 V [6]. The applications of GaN power devices are focused on wireless power transmission [7], switched-mode power supplies [8], and microinverters [9]. For SiC power devices, the voltage rating is typically in the range of 600~1700 V and high thermal conductivity allows good thermal performance [10–12]. The applications are mainly focused on renewable power conditioning systems [13], electric vehicles, and medium-voltage motor drives [14].

Multilevel converters have the general advantages of improved efficiency, lower dv/dt and di/dt, reduced harmonics, reduced EMI, lower common mode current, and the advantages of transformerless and fault-tolerant operations [15–20]. This class of converters is used in high or medium voltage, high power (multi-MWs) applications, including induction and synchronous motor drives for various industrial applications, high voltage DC systems, flexible AC transmission systems (FACTS), static VAR compensators, photovoltaic and wind generation systems, unmanned aerial vehicles (UAVs), etc. Generally, multilevel inverters are used for medium voltage applications to divide high voltage into smaller voltage steps [21]. The application of multilevel inverters can be extended to the 560~750 V voltage range due to the development of power semiconductors such as SiC and GaN, returning lower conduction and switching losses, higher energy efficiency with respect to the classical two-level inverter. Additional benefits of multilevel topologies are the reduction of voltage transients at the motor windings especially with long shielded motor cables, reduced stresses on the power switches, lower harmonic distortion content in the output voltage and current, and smaller output filter and inverter size. Since electric mobility applications require high power density, high efficiency, and a wide range of batteries, multilevel inverters are good candidates for these applications.

The work in [22] presents a comparison of conduction and switching losses of Si-IGBT, SiC-MOSFET and GaN devices in a 3-phase 3-level diode clamped inverter fed induction motor drive. The work in [23] proposes a front-end isolated quasi-Z-source cascade multilevel inverter for PV grounding issues, and it compares the SiC and GaN MOSFETs performance. A comparison of the efficiency of GaN and SiC devices in two-level and three-level converters considering different modulation techniques has been considered in [24]. In [25], an overview of the performance of various power switches in multilevel inverters has been presented. The analysis has shown that MOSFETs are better for low-power applications while IGBTs are suitable for high-power applications and GaN devices are promising for developing high-frequency multilevel inverters in the next future. However, there is no device comparison in multilevel converter that could be used for UAV. Hence, the paper analyzes five-level cascaded H-bridge inverters equipped with power semiconductors Si, SiC MOSFET, GaN HEMT, and IGBT in the range of input power 500–8000 W and calculates the power losses when the switching frequency varies between 400 Hz and 20 kHz. A further comparison between wide bandgap devices has been performed at 100 kHz. The goal of this study is to give a guide for the choice of the devices to be used in the 5-level inverter depending on different UAV operation scenarios.

2. Reference scheme working at a fundamental switching frequency

As a reference scheme, a 5-level cascaded H-bridge (CHB) inverter (Figure 1) built with ideal switches is considered and a selective harmonic elimination (SHE) procedure operating at a fundamental switching frequency equal to 400 Hz is proposed [26].

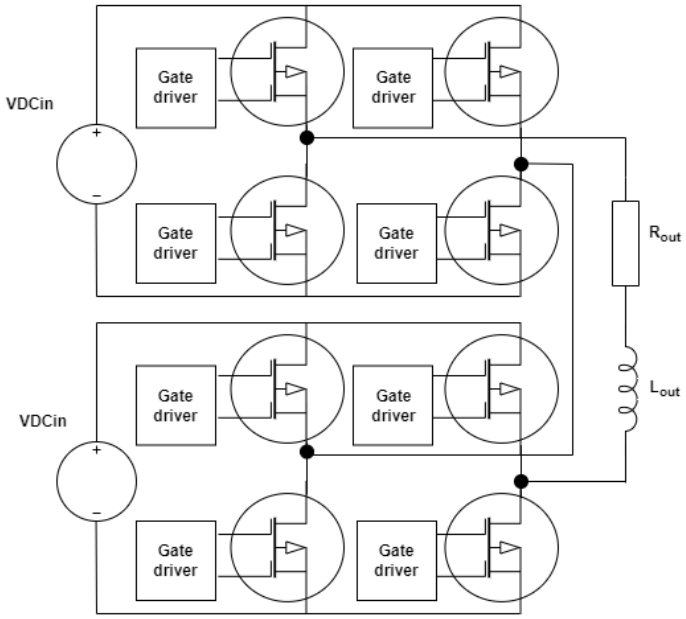

Figure 1. CHB 5-level inverter configuration.

This procedure analytically computes the switching angles. It starts with the Fourier series expansion of output phase voltage V_{out} as:

$$v_{out} = \sum_{k=1,3,5,7,\ldots}^{+\infty} H_k \, sin(k\omega t) \tag{1}$$

where H_k is the amplitude of the kth harmonic

$$H_k = \frac{4V_{dcin}}{\pi k}[cos(k\alpha_1) + cos(k\alpha_2)] \tag{2}$$

where V_{dcin} is the DC voltage input and (α_1, α_2) the unknown switching angles, which have to satisfy the following constraint:

$$0 \leq \alpha_1 \leq \alpha_2 \leq \frac{\pi}{2} \tag{3}$$

To eliminate the third harmonic and its multiple, the following system has to be solved:

$$\begin{cases} cos(3\alpha_1) + cos(3\alpha_2) = 0 \\ cos(\alpha_1) + cos(\alpha_2) = 2m \end{cases} \tag{4}$$

where $m = \frac{H_1 \pi}{8V_{dcin}}$ the modulation index and H_1 is the fundamental harmonic amplitude.

The equation system (4), by applying the Prostaphaeresis formulas, can be rewritten as:

$$\begin{cases} cos\left(3\frac{\alpha_1+\alpha_2}{2}\right) + cos\left(3\frac{\alpha_1-\alpha_2}{2}\right) = 0 \\ cos\left(\frac{\alpha_1+\alpha_2}{2}\right) + cos\left(\frac{\alpha_1-\alpha_2}{2}\right) = 2m \end{cases} \tag{5}$$

giving

$$\begin{cases} \alpha_1 + \alpha_2 = \frac{\pi}{3} \\ \alpha_1 - \alpha_2 = 2arccos\left(\frac{m}{cos\left(\frac{\pi}{6}\right)}\right) \end{cases} \tag{6}$$

That in matrix form is

$$\begin{gathered} [\boldsymbol{A}][\boldsymbol{\alpha}] = [\boldsymbol{b}] \\ with \\ [\boldsymbol{A}] = \begin{bmatrix} 1 & 1 \\ 1 & -1 \end{bmatrix} \\ [\boldsymbol{\alpha}] = \begin{bmatrix} \alpha_1 \\ \alpha_2 \end{bmatrix} \\ [\boldsymbol{b}] = \begin{bmatrix} \frac{\pi}{3} \\ 2arccos\left(\frac{m}{cos\left(\frac{\pi}{6}\right)}\right) \end{bmatrix} \end{gathered} \tag{7}$$

Observing that the inverse of the matrix $[\boldsymbol{A}]^{-1} = \frac{[\boldsymbol{A}]}{2}$, since $[\boldsymbol{A}]^2 = 2[\boldsymbol{I}]$ and $[\boldsymbol{I}]$ is the identity matrix, the vector of switching angles $[\boldsymbol{\alpha}]$ can be computed by the product $[\boldsymbol{\alpha}] = [\boldsymbol{A}]\frac{[\boldsymbol{b}]}{2}$.

The obtained switching angles eliminating the third harmonics and its multiple, depending on the modulation index, are shown in Table 1. Figures 2, 3, and 4 show the harmonic spectrum obtained by the previous switching angles for m = 0.8, 0.7 and 0.5, respectively.

The total harmonic distortion (THD), including the harmonics up to the forty-ninth, can be computed as:

$$THD = \frac{\sqrt{\sum_{k=3,5,7,\ldots}^{49}\left[\frac{cos(k\alpha_1)+cos(k\alpha_2)}{k}\right]^2}}{|cos(\alpha_1)+cos(\alpha_2)|} \tag{8}$$

For switching frequencies higher than the fundamental one, simulations are carried out by using the phase-shifted (PS) carrier modulation technique. The major advantage of this scheme over level-shifted and space vector modulation schemes is its inherent ability to evenly distribute losses between semiconductor devices. Its implementation requires a capacitor voltage balancing scheme. For the CHB 5-level inverter, the carrier signals of the two cells, which are equal in amplitude and

frequency, are phase-shifted by $\pi/2$. The PS scheme allows shifting the voltage harmonics towards high frequencies that depend on the switching frequency f_{sw}. More specifically, the generated harmonics are centred at frequencies $f = 4 \cdot k \cdot f_{sw}$, $k = 1, 2, \ldots$

Table 1. Switching angles obtained by SHE.

m	α_1[rad]	α_2[rad]
0.45	0.5008	1.5480
0.50	0.4317	1.4789
0.55	0.3591	1.4063
0.60	0.2818	1.3290
0.65	0.1983	1.2455
0.70	0.1060	1.1532
0.75	0.0000	1.0472
0.80	0.1306	0.9166
0.85	0.3309	0.7163

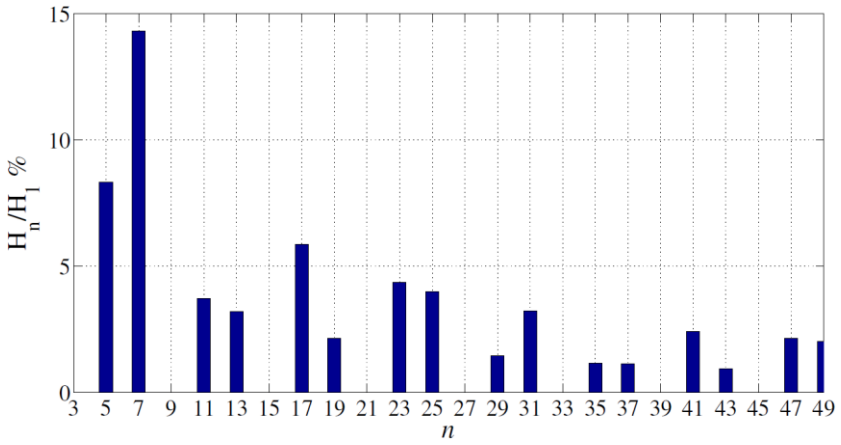

Figure 2. Harmonic analysis obtained for the reference scheme for m = 0.8.

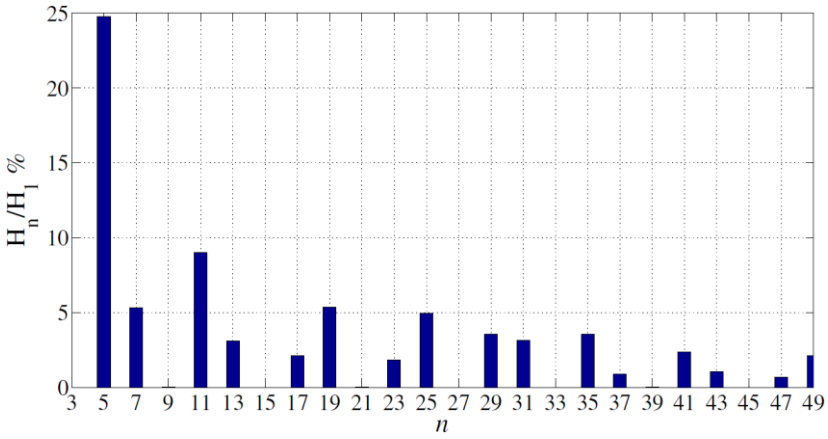

Figure 3. Harmonic analysis obtained for the reference scheme for m = 0.7.

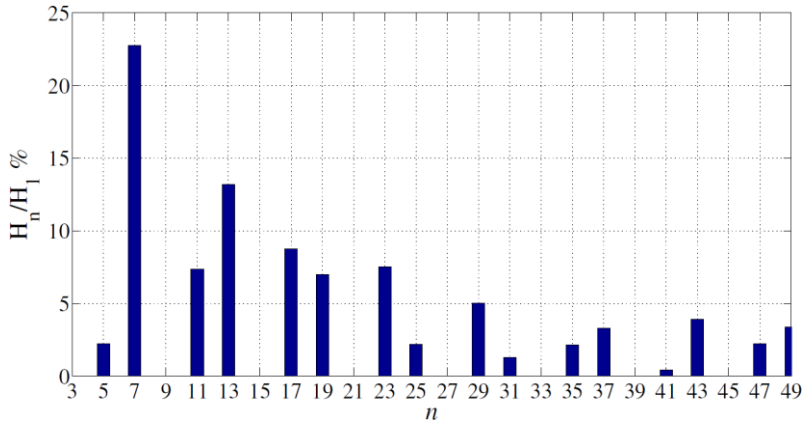

Figure 4. Harmonic analysis obtained for the reference scheme for m = 0.5.

3. Analysis of five-level CHB inverter considering real switch circuit models

3.1. Circuit models and simulation setup

In this work, power devices with different structures and technology have been tested. They are listed in Table 2. The power devices have been chosen with similar breakdown voltage (600–650 V) and on-state resistance ($R_{DS,on}$), that is 48 mΩ at room temperature. The IGBT has been selected considering the forward on-voltage (V_F) when the maximum current flows through it in this application. In detail, the ratio between the V_F and this current (approximately 30 A) is similar to the $R_{DS,on}$ of the other devices in Table 2.

Table 2. Devices considered in the comparison.

Device	Manufacturer	Code
Si MOSFET	STMicroelectronics	STO67N60DM6 [27]
SiC MOSFET	Infineon	IMZA65R048M1H [28]
GaN HEMT	GaNSystem	GS-065-030-2-L [29]
IGBT	STMicroelectronics	STGWA60V60DWFAG [30]

For each power device, a gate driver circuit has been implemented to optimize the switching waveforms. In Figure 5, a generic gate driver used for the simulations has been reported.

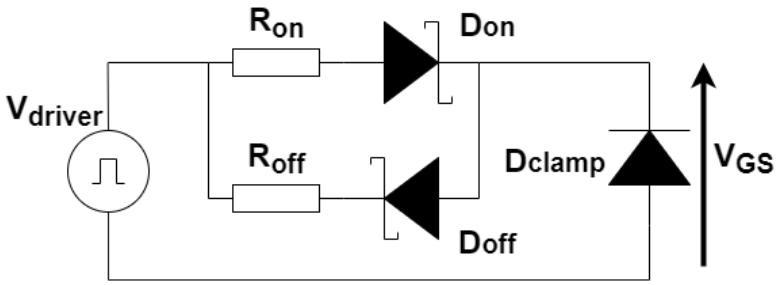

Figure 5. Generic gate driver adopted for the simulations.

In the gate driver, R_{on} and R_{off} enable the regulation of the turn-on and turn-off slew rates, respectively. These regulations are important to avoid positive and negative glitches in the complementary devices. In fact, the former could involve an undesired turn-on which involves shorting the leg, while the latter could destroy the oxide of the complementary device. Moreover, as the value of these resistances increases it is less probable the overlapping of the V_{GS} of the devices of the same leg during a commutation. Considering that the GaN device is the fastest one R_{on} was initially set to 20 Ω according to usual rules [31]. However, during the simulations, the positive glitch on the gate-source voltage of the off-state device (due to the turn-on of the complementary device) involved its undesired turn-on causing leg shoot-through. Therefore, the value has increased to 25 Ω. Although a lower value could be considered for the others, it has been preferred to adopt the same value of R_{on} to perform the comparison at equal external conditions. Similarly, the R_{off} value has been set. The same R_{on} (25 Ω) and R_{off} (3.3 Ω) were used for all power devices. D_{on} and D_{off} are used as resistor selectors. The first allows the current to flow only when the device is turning on, while the second enables the current path during the turn-off. They present a forward voltage (FV) equal to 0.3 V. The diode connected between the gate and kelvin is a clamp diode with an FV equal to 1.5 V. This component avoids excessive negative V_{GS} voltage on the complementary device to the turning-on one to avoid oxide damage.

As mentioned before, the simultaneous switching of two devices on the same leg must be avoided. Hence, an adequate blanking time has been used considering the specific device features and the previous choice of the resistors R_{on} and R_{off}. Table 3 reports the blanking time adopted in the driver for the converter control according to the adopted device as well as the related on and off voltage.

As faster the power device switches the smaller the blanking time. Moreover, other aspects must be considered. A proper blanking time must be considered in a device subject to the reverse phenomenon especially when it has a large negative impact. More specifically, a Si MOSFET is affected by the reverse recovery of its parasitic body diode, while the GaN HEMT does not have a reverse recovery time because it has not an intrinsic body diode. In Figure 6 the switching of the considered GaN HEMT is reported. In this simple case, the considered blanking time is largely sufficient.

The output of the multilevel converter has been modelled with an R_L load. The value of the input voltage V_{DCin} is set to 283 V. The schematic of the simulated multilevel converter has been reported in Figure 1, where the gate driver mentioned in the boxes is the one shown in Figure 5.

Simulations with different power outputs have been performed. In Table 4, the simulation of the different conditions has been reported. These simulations have been first performed considering SHE, which is a switching frequency equal to the fundamental one, i.e. 400 Hz, which is typical in this application.

Table 3. Parameters set in the pulse voltage source (V_{driver}).

	V_{driver} min [V]	V_{driver} max [V]	Blanking time [ns]
Si MOSFET	0	10	400
SiC MOSFET	0	18	100
GaN HEMT	0	6	50
IGBT	0	15	600

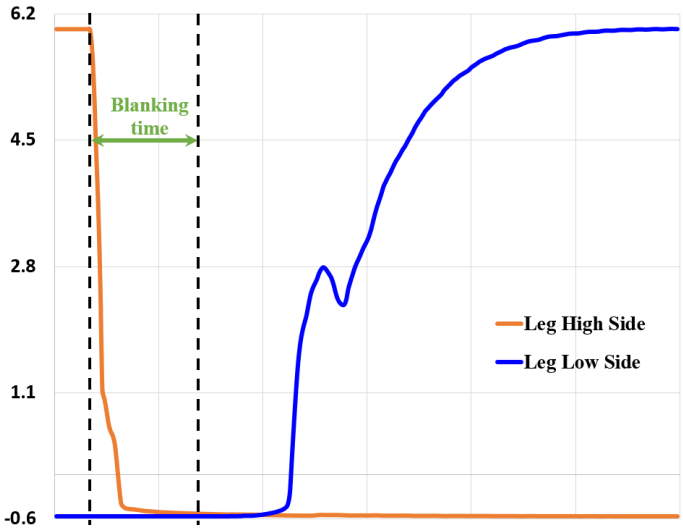

Figure 6. Switching of the GaN HEMT.

Moreover, other simulations have been performed considering PS carrier modulation techniques: 4 kHz and 20 kHz to account for the operating frequency of the IGBT. A further comparison between wide bandgap devices has been performed at 100 kHz. The simulations have been carried out with SIMetrix software using the circuit model provided online by the devices manufacturers. They are typically Spice-like circuit model of the power devices [32–37].

Table 4. Simulation conditions.

Output power [W]	I_{out} [A]	R_{out} [Ω]	L_{out} [μH]
500	1.7	388	16.3
1000	3.5	194	16.3
2000	7	96.5	16.3
5000	17.6	38.3	16.3
8000	28.2	23.7	16.3

3.2. Simulation results

The modulation index of the adopted SHE has been set to m = 0.85. In Figures 7–10, the relationship between input power and power losses as the switching frequency varies has been graphed. For each figure, there are four curves: a blue curve for GaN HEMT, a red curve for SiC MOSFET, a green curve for Si MOSFET, and a light blue curve for IGBT.

When SHE modulation is adopted (i.e., at the fundamental frequency, 400 Hz) until 50% of the full load, the GaN HEMT and the MOSFETs (Si, SiC) present the same performance, which is better than the IGBT one and the gap increases as the load increases (Figure 7).

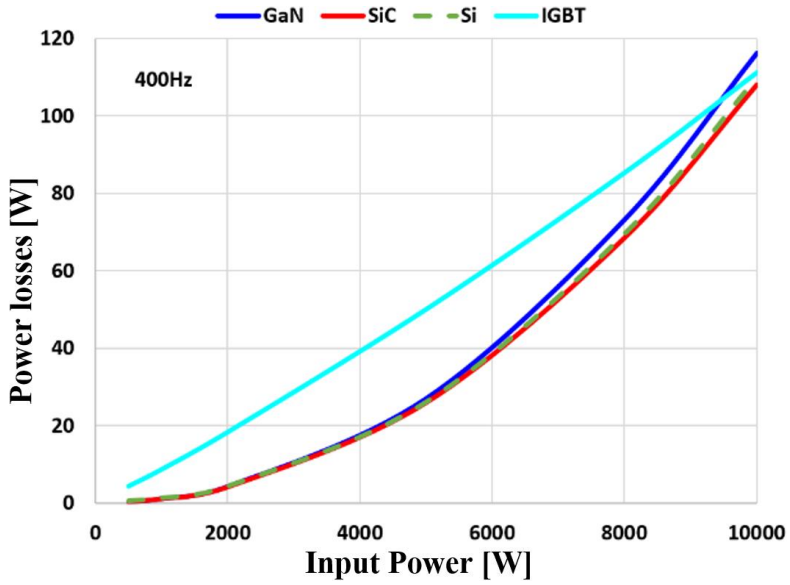

Figure 7. Power losses of Si and wide-bandgap devices at 400 Hz.

From 50% of the full load, the performance of GaN is worse in comparison to the MOSFETs (Si, SiC), which present the best performance although the SiC MOSFET slightly outperforms the Si one, especially at high load. In this case, the performance of the IGBT is the worst almost always because, differently from the previous case, the gap decreases as the load increases. Indeed, at full load, the IGBT tends to the SiC MOSFET while the GaN device presents the highest losses. Considering that IGBT devices present the lowest cost and a Si MOSFET costs less than a wide-bandgap device, the following conclusion can be derived. The IGBT is the first choice only if the converter mainly operates at full load. This occurs in applications where the UAV is often used at maximum performance, such as flying at high speed or frequently climbing and descending. Otherwise, the higher cost of Si MOSFET should be faced when the converter operates differently. This condition occurs when the UAV is used at the maximum load only in a few intervals (i.e., during the take-off, climb, and landing phase) while rarely it is forced at maximum speed during the cruise and rarely it has to climb and descend during its operation. Therefore, the choice must account for the typical working conditions of the specific application.

In conclusion, regardless of the UAV usage and consequently the converter operation, the use of wide-bandgap devices should be avoided since there is not any performance improvement that justifies a greater cost.

In the case of the PS carrier modulation technique at 4 kHz (Figure 8), there are some differences from the previous case. In this case, the switching frequency is 4kHz since, differently from the previous case, it depends on the carrier frequency. Until 50% of the full load, the GaN HEMT and the SiC MOSFETs present about the same losses, which is better than the Si MOSFET while the IGBT is the worst one. The gap between the Si MOSFET and the wide-bandgap devices is almost constant (increases very slightly) while, as before, the gap with IGBT losses increases with increasing load. From 50% of the full load, the performance of GaN HEMT is worse in comparison to the SiC MOSFET and the gap slightly increases as the load increases.

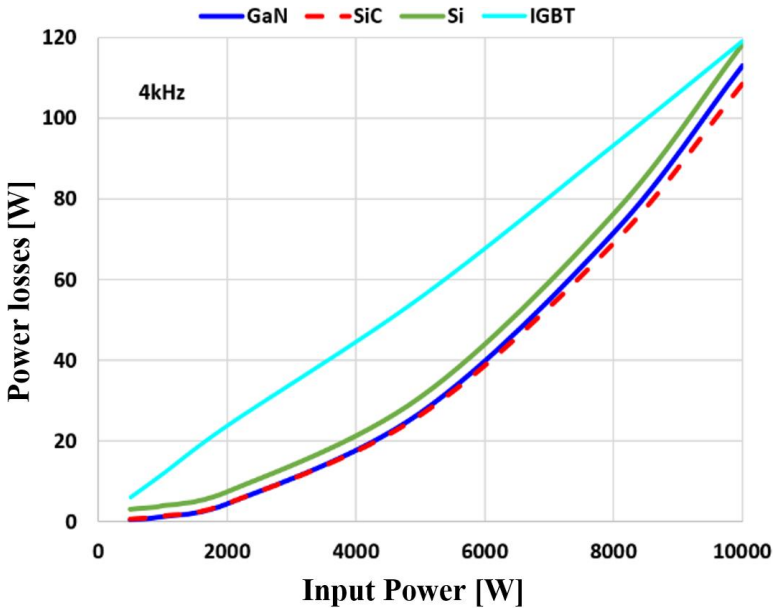

Figure 8. Power losses of Si and wide-bandgap devices at 4 kHz.

Also, in this case, the performance of Si MOSFET is worse than the wide-bandgap devices and the gap slightly increases reaching the maximum gap at the full load. Similar to the previous case, the gap between the power losses of the IGBT and of the other devices reduces as the load increases. On the other hand, differently from before, it performs worse than both wide-bandgap devices also at full load. In this condition, both Si devices present about the same power losses. The IGBT should be totally avoided if the power losses are the main selection criterion. The use of Si MOSFETs could be considered if it is expected that often the converter will be operated at low load (until 50%) since the reduced cost compensates for the small additional losses. This condition occurs when the converter operates at a high load during the ascending and descending period while mainly flying slowly. Otherwise, as the average UAV cruise speed increases or frequently climbs and descends to perform the specific application tasks, the loss gap between Si and SiC MOSFETs increases thus the higher cost of the latter MOSFET should be faced.

In conclusion, regardless of the UAV usage and consequently the converter operation, the use of IGBT should be avoided due to the bad performance, while the use of GaN HEMT devices must be avoided since they cost more than SiC MOSFETs without performing better.

In the case of the PS carrier modulation technique, carrier at 20 kHz (i.e., the switching frequency), the results reported in Figure 9 show that the considerations about the IGBT and Si MOSFET when compared with the wide-bandgap devices are like the 4 kHz case. The main difference consists in the strongly increased gap between Si and wide-bandgap devices. In this case, the two kinds of wide-bandgap devices present the same performance regardless of the power level. Therefore, considering the higher cost of GaN HEMT devices, the SiC MOSFET is the best choice.

According to these results, it is expected that if the switching frequency increases the gap between Si and wide-bandgap devices increases and, consequently, the use of Si devices should be avoided. Therefore, only the wide-bandgap devices have been simulated in the case of the PS carrier modulation technique, carrier at 100 kHz (Figure 10). Indeed, regardless of the power losses, the use of IGBT would be not possible since this frequency is out of its capability.

The results show that in this case, the GaN HEMT outperforms the SiC MOSFET regardless of the load. However, until 50% of the full load the improvement achievable using the GaN HEMT is negligible. However, considering the trend (Figures 9,10), it is expected that the gap becomes significant as the switching frequency increases. From 50% of the full load, the performance of SiC MOSFET is worse in comparison to the GaN HEMT and the difference increases as the load increases.

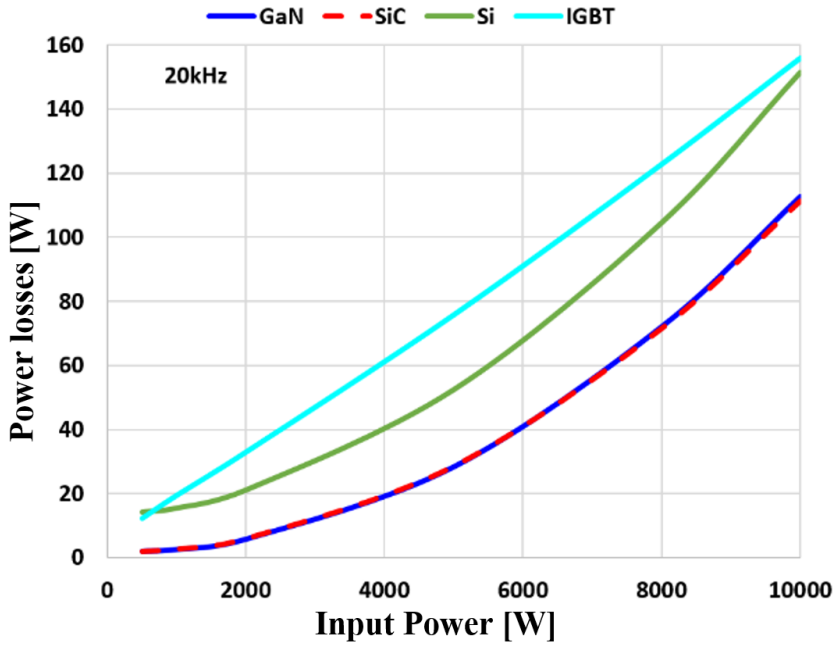

Figure 9. Power losses of Si and wide-bandgap devices at 20 kHz.

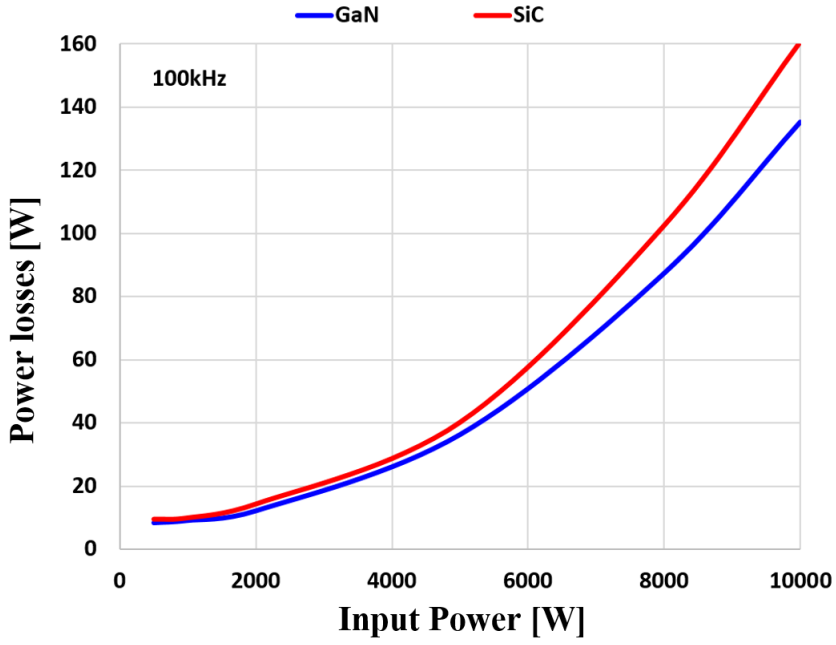

Figure 10. Power losses of wide-bandgap devices at 100 kHz.

Considering that SiC MOSFETs present a lower cost than GaN HEMT, the following conclusion can be derived. The GaN HEMT is the first choice when the converter mainly operates medium or large loads. This occurs when the UAV is often used at maximum performance, by flying at medium or high speed or by frequently climbing and descending to perform specific application tasks. Otherwise, one can benefit from the lower cost of SiC MOSFETs when the converter operates in a different manner. In particular, in applications where the UAV is used at a high load only in a few intervals, e.g., take-off and landing phase, while usually the cruise speed is low and rarely it climbs and descends during its operation.

In conclusion, when a high switching frequency is considered, the GaN HEMT is usually the best choice.

Figure 11 reports the amplitudes of the harmonic normalized with respect to the fundamental one when the circuit model of the switches is adopted. In particular, they are expressed in percentage of the amplitude of the fundamental component of the output voltage spectrum. The results are obtained for the case 8 kW when the modulation index is equal to 0.85 and using the PS carrier modulation technique with a carrier at 20 kHz. The related power losses of the 4 kinds of devices are reported in Figure 9. Figure 11(a) reports the normalized amplitude of the odd harmonics until the 49-th related to the output voltage. The third harmonic and its multiple appear in the figure differently from the ideal case where they are zero (see Figures 2–4). However, their amplitude is low; a magnification of them is reported in Figure 11(b). From the analysis of this figure is evident that the Si MOSFET is the worst device because the output voltage, generated when it is used, presents an amplitude of these 3-rd and its multiples are much larger than when the other devices are used. On the contrary, the SiC MOSFET presents the best performance, thus consolidating its leading position in the case of PS carrier modulation technique with carrier at 20 kHz.

The normalized amplitude reported in Figure 11(a) for the actual devices has been compared with the ideal ones that would be obtained in the case of ideal switches. The comparison has been performed for the non-zero harmonics of the ideal output voltage spectrum (i.e., the 3-rd and its multiples are not considered). The error, $E_{d,k}$, on the k-th harmonic due to the use of a non-ideal switch, *d*, has been computed according to the following equation:

$$E_{d,k} = \frac{\frac{H_{d,k}}{H_{d,1}} - \frac{H_k}{H_1}}{\frac{H_k}{H_1}} \% \tag{9}$$

where $H_{d,1}$ and $H_{d,k}$ represent the amplitude of the fundamental and the k-th output voltage harmonic, respectively, obtained by simulation using the device *d* (Si MOSFET, SiC MOSFET, GaN HEMT and IGBT); while H_1 and H_k represent the same quantities for the ideal switches.

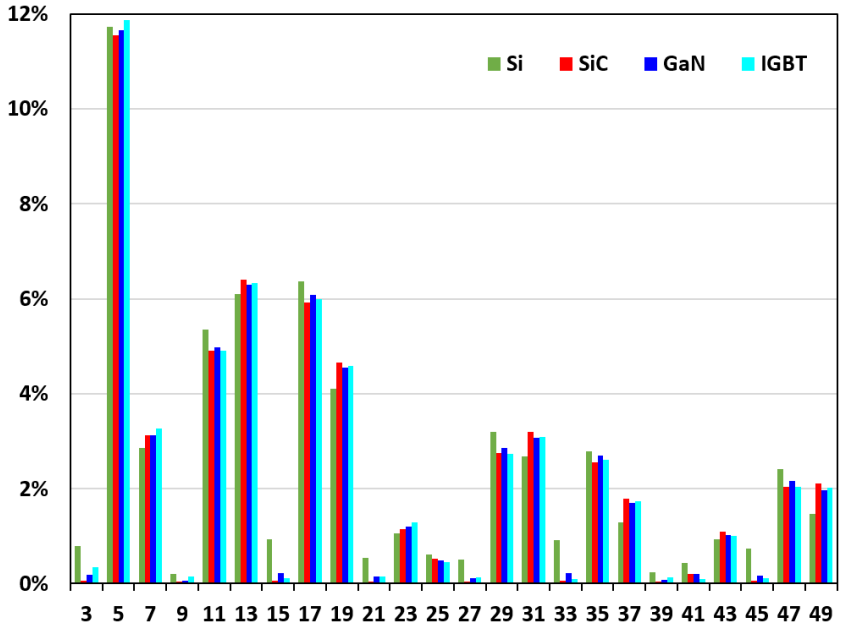

(a)

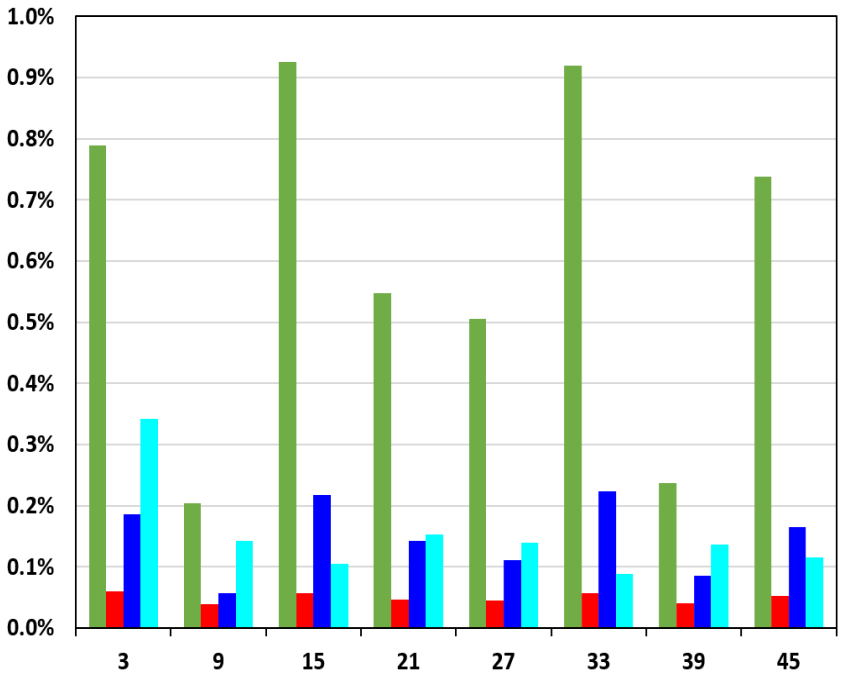

(b)

Figure 11. Normalized harmonic amplitudes when the circuit model of the devices is adopted: load equal to 8 kW. (a) Odd harmonics until the 49th; (b) third harmonic and its multiple—(they are ideally zero).

Figure 12 reports the values of $E_{d,k}$. As evident from Figure 12(a), once again, the Si MOSFET provides the worst results. Except for the IGBT, all the other devices present a large estimation error for the 41-th harmonic. Figure 12(b) reports a magnification of the results in Figure 12(a). In the last are removed the errors greater than 30% (i.e., results related to the 25-th harmonic for Si MOSFET and 41-th harmonic for GaN HEMT, Si and SiC MOSFET). Figure 12(b) confirms that Si MOSFET performs worse than the other devices. The IGBT is better at looking at the results as a whole.

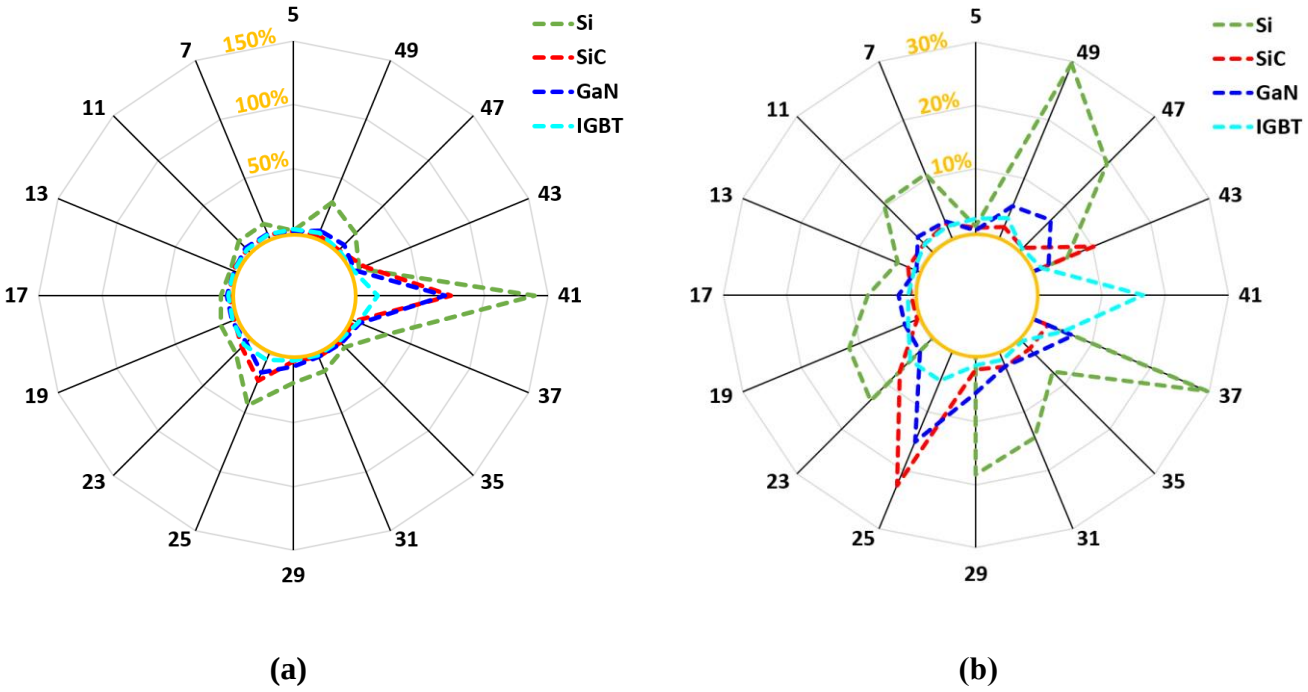

Figure 12. Estimation error (the orange circle represents zero error for each harmonic). (a) Overall view; (b) magnification until the 30% error (errors larger than 30% are removed).

Figure 13 reports the amplitudes of the harmonic normalized with respect to the fundamental one when the circuit model of the switches is adopted. In particular, they are expressed in percentage of the amplitude of the fundamental component of the output voltage spectrum. The results are obtained for the case 2 and 5 kW when the modulation index is equal to 0.85 and using the PS carrier modulation technique with a carrier at 20 kHz. The results are similar to the ones reported in Figure 11, thus, similar conclusions hold.

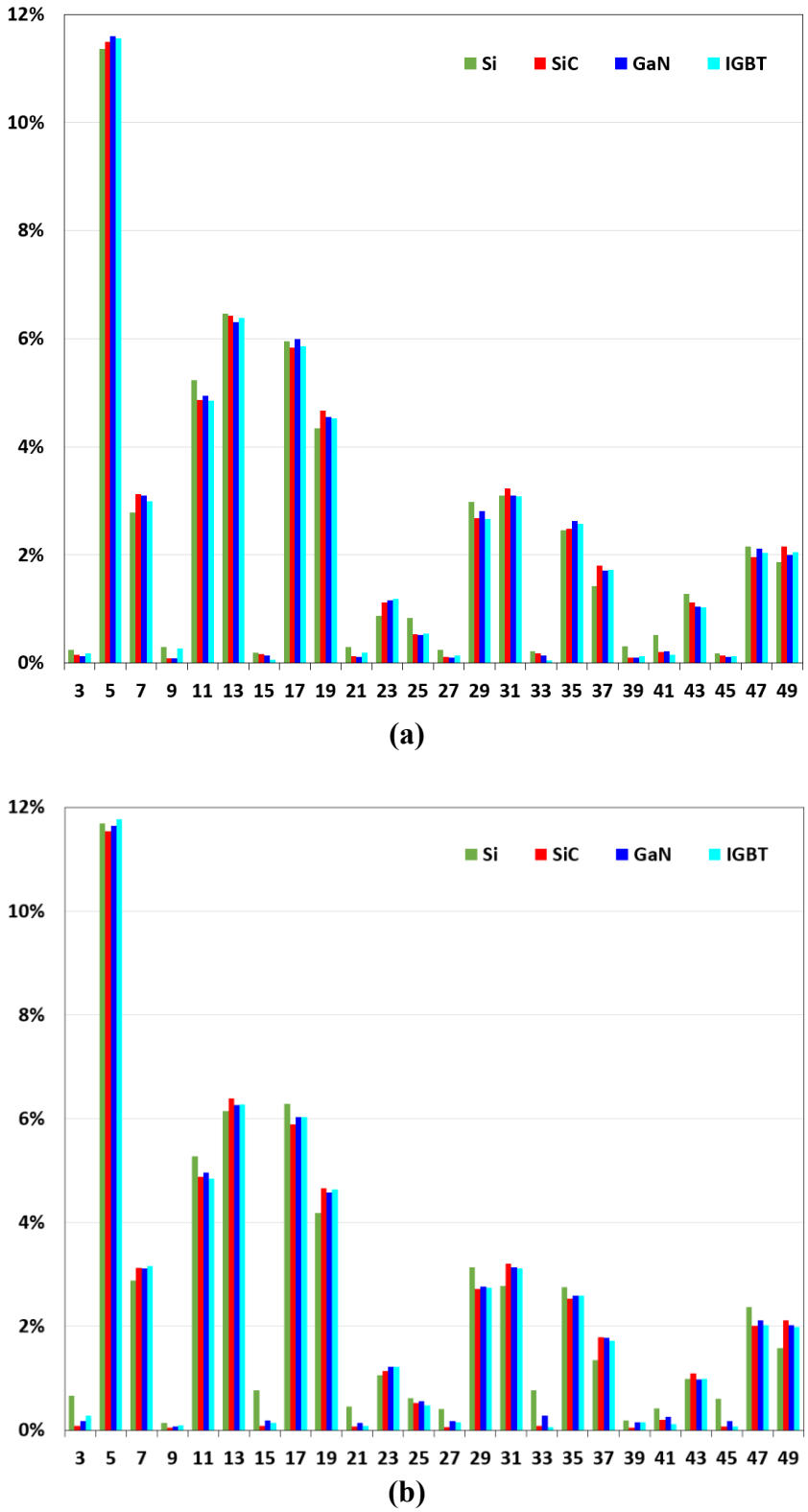

Figure 13. Normalized harmonic amplitudes when the circuit model of the devices is adopted. (a) 2 kW; (b) 5 kW.

4. Conclusions

In this paper, a 5-level cascaded H-bridge inverter and the related modulation have been considered for UAV applications. More specifically, different operation scenarios considering typical operations, such as take-off, climb, land, and cruise, as well as potential recurring climbs and descents, have been considered to account for different application targets. The converter and the proposed modulation techniques have been simulated using circuit models of the converter and IGBT, GaN HEMT, and Si and SiC MOSFET. The results have highlighted that in the case of a selective harmonic elimination procedure operating at the fundamental switching frequency, the Si devices should be used. More specifically, IGBTs should be considered only when the converter frequently operates at full load. Otherwise, the Si MOSFET should be adopted although it involves increased cost, while additional wide bandgap devices are useless due to the lack of performance improvement. In the case of the phase-shifted carrier modulation technique, at 4 kHz the MOSFET is the best device and preferring the Si or SiC devices depends on the UAV usage. More specifically, at the load is GaN HEMT and the SiC MOSFETs present about the same losses, which is a few better than the Si MOSFET while the IGBT is the worst one. The gap between the Si MOSFET and the wide-bandgap devices is almost constant (increases very slightly) while, as before, the gap with IGBT losses increases with increasing load. From 50% of the full load, the performance of GaN HEMT is worse in comparison to the SiC MOSFET and the gap slightly increases as the load increases. At 20 kHz the SiC MOSFET is the best device, while at high frequency the GaN HEMT cost should be faced to take advantage of its best performance.

Use of AI tools declaration

The authors declare that they have not used any AI tools.

Author contributions

The authors declare that they equally contribute to the paper.

Acknowledgments

The work has been supported in part by the project “Advanced power-trains and systems for full electric aircrafts—2017MS9F49” funded by the “Ministero dell'Istruzione dell'Università e della Ricerca” under the call PRIN 2017.

Conflict of interest

The authors declare no conflicts of interest. Santi Agatino Rizzo is an editorial board member for AIMS Energy and was not involved in the editorial review or the decision to publish this article. All authors declare that there are no competing interests.

References

1. Yang K, Feng M, Wang Y, et al. (2019) Real-time switching angle computation for selective harmonic control. *IEEE Trans Power Electron* 34: 8201–8212. https://doi.org/10.1109/TPEL.2018.2881448
2. Faizan M, Wang X, Yousaf MZ (2023) Design and comparative analysis of an ultra-highly efficient, compact half-bridge LLC resonant GaN converter for low-power applications. *Electronics* 12: 2850. https://doi.org/10.3390/electronics12132850
3. Sun P, Zou M, Wang Y, et al. (2023) Focuses and concerns of dynamic test for wide bandgap device: A questionnaire-based survey. *IEEE Trans Power Electron* 38: 15522–15534. https://doi.org/10.1109/TPEL.2023.3312563
4. Ilves K, Harnefors L, Norrga S, et al. (2015) Analysis and operation of modular multilevel converters with phase-shifted carrier PWM. *IEEE Trans Power Electron* 30: 268–283. https://doi.org/10.1109/TPEL.2014.2321049
5. Joshi V, Pande P, Jadli U, et al. (2023) Impact of parasitic elements on the power dissipation of Si superjunction MOSFETs, SiC MOSFETs, and GaN HEMTs. *Eng Res Express* 5: 035077. https://doi.org/10.1088/2631-8695/acf97d
6. Zhong K, Wang Y, Lyu G, et al. (2022) 650-V normally-off GaN/SiC cascode device for power switching applications. *IEEE Trans Ind Electron* 69: 8997–9006. https://doi.org/10.1109/TIE.2021.3114697
7. Sulistyo M, Pradhityo G, Muharam A, et al. (2023) Modeling high frequency 13.56 MHz Full bridge inverter based on GaN MOSFET for EV wireless charging system. *Evergreen* 10: 1847–1854. https://doi.org/10.5109/7151734
8. Neeraja K, Bhavya Y, Mohan S, et al. (2016) Design, simulation and implementation techniques of high performance GaN SMPS. *IEEE International Conference on Power Electronics, Drives and Energy Systems (PEDES)*, Trivandrum, India. https://doi.org/10.1109/PEDES.2016.7914396
9. Zakzewski D, Resalayyan R, Hasnain A, et al. (2023) Controller verification of a smart-grid compatible 200 kHz single-stage photovoltaic microinverter. *IEEE Applied Power Electronics Conference and Exposition (APEC)*, Orlando, FL, USA. https://doi.org/10.1109/APEC43580.2023.10131580
10. Isa R, Mirza J, Ghafoor S, et al. (2023) Junction temperature optical sensing techniques for power switching semiconductors: A review. *Micromachines* 14: 1636. https://doi.org/10.3390/mi14081636
11. Hwang D, Joo D, Gu B (2024) Analysis of inverter loss improvement according to Si-IGBT and SiC-MOSFET utilization of 150kW inverter for EV propulsion. *Trans Korean Inst Electr Eng* 73: 63–68. https://doi.org/10.5370/KIEE.2024.73.1.63
12. Li B, Yang R, Xu D, et al. (2015) Analysis of the phase-shifted carrier modulation for modular multilevel converters. *IEEE Trans Power Electron* 30: 297–310. https://doi.org/10.1109/TPEL.2014.2299802
13. Villanueva I, Vázquez N, Vaquero J, et al. (2023) Photovoltaic inverter reliability study through sic switches redundant structures. *Technologies* 11: 59. https://doi.org/10.3390/technologies11020059

14. Alatise O, Deb A, Bashar E, et al. (2023) A review of power electronic devices for heavy goods vehicles electrification: performance and reliability. *Energies* 16: 4380. https://doi.org/10.3390/en16114380
15. Carrasco-González D, Horrillo-Quintero P, García-Triviño P, et al. (2024). Control of PV power plants with quasi-Z-source cascaded H-bridge multilevel inverters under failure. *Int Electr Power Energy Syst*, 157. https://doi.org/10.1016/j.ijepes.2024.109803
16. Sivarajeswari S, Hublikar S, Kumar Y, et al. (2024) Multiple level inverter scheme for improved power quality of renewable energy solar panel. *Int J Intell Syst Appl Eng* 12: 98–105. Available from: https://ijisae.org/index.php/IJISAE/article/view/3398.
17. Gao S, Chen Y, Song Y, et al. (2024) An efficient half-bridge MMC model for emtp-type simulation based on hybrid numerical integration. *IEEE Trans Power Syst* 39: 1162–1177. https://doi.org/10.1109/TPWRS.2023.3262584
18. Sheng J, Xiang X, Li B, et al. (2023) High-Efficient operation for modular multilevel resonant DC–DC converters in medium voltage applications with wide input range and wide load condition. *IEEE Trans Power Electron* 38: 12180–12194. https://doi.org/10.1109/TPEL.2023.3295828
19. Muthukaruppasamy S, Parimalasundar E, Rajagopal V, et al. (2023) Integrating MPPT and artificial neural networks for efficient DC-DC and DC-AC conversion in photovoltaic applications. *SSRG Int J Electr Electron Eng* 10: 51–61. https://doi.org/10.14445/23488379/IJEEE-V10I8P105
20. Babaie M, Al-Haddad K (2023) Self-Training intelligent predictive control for grid-tied transformerless multilevel converters. *IEEE Trans Power Electron* 38: 12482–12496. https://doi.org/10.1109/TPEL.2023.3293820
21. Buccella C, Cecati C, Cimoroni M, et al. (2014) Analytical method for pattern generation in five-level cascaded H-bridge inverter using selective harmonic elimination. *IEEE Trans Ind Electron* 61: 5811–5819. https://doi.org/10.1109/TIE.2014.2308163
22. Dutta S, Yadav A (2023) Power loss comparison of Si-IGBT SiC-MOSFET and GaN Based 3-level diode clamped inverter fed induction motor drive. *IEEE International Conference on Power Electronics, Smart Grid, and Renewable Energy (PESGRE)*, Trivandrum, India. https://doi.org/10.1109/PESGRE58662.2023.10405187
23. Liu Y, Ge B, Abu-Rub H, et al. (2016) Comparison of SiC and GaN devices for front-end isolation of quasi-Z-source cascaded multilevel photovoltaic inverter. *IEEE Energy Conversion Congress and Exposition (ECCE)*, Milwaukee, WI, USA. https://doi.org/10.1109/ECCE.2016.7854942
24. Najjar M, Nymand M, Kouchaki A, et al. (2021) Efficiency comparisons of two-level and three-level GaN/SiC based converters. *IEEE 12th Energy Conversion Congress & Exposition—Asia (ECCE-Asia)*, Singapore, 13–18. https://doi.org/10.1109/ECCE-Asia49820.2021.9479380
25. Suryawanshi A, Chopade N, Mehta H (2021) Micro-controllers and power devices used in multilevel inverters—A Survey. *International Conference on Green Energy, Computing and Sustainable Technology (GECOST)*, Miri, Malaysia, 1–5. https://doi.org/10.1109/GECOST52368.2021.9538707
26. Buccella C, Cecati C, Cimoroni M, et al. (2017) A selective harmonic elimination method for five-level converters for distributed generation. *IEEE J Emerg Select Topic Pow Elec* 5: 775–783. https://doi.org/10.1109/JESTPE.2017.2688726
27. Spice model of the device STO67N60DM6. Available from: https://www.st.com/resource/en/spice_model/sto67n60dm6_spice.zip.

28. Spice model of the device IMZA65R048M1H. Available from: https://www.infineon.com/dgdl/Infineon-CoolSiC_silicon_carbide_MOSFET_650V_SPICE-SimulationModels-v05_00-EN.zip?fileId=5546d4626fc1ce0b016fc742477d0bb1.
29. Spice model of the device GS-065-030-2-L. Available from: https://gansystems.com/wp-content/uploads/2021/08/GS-650-030-2-L-Spice-Models-V3P2.rar.
30. Spice model of the device STGWA60V60DWFAG. Available from: https://www.st.com/en/power-transistors/stgwa60v60dwfag.html#cad-resources.
31. What is the recommended gate resistance to start with? Available from: https://gansystems.com/gan-transistors/faq/#toggle-id-12.
32. Zarębski J, Bisewski D (2023) The modeling of GaN-FET power devices in SPICE. *Energies* 16: 7643. https://doi.org/10.3390/en16227643
33. Er-Rafii H, Galadi A (2023) An optimal parameter extraction procedure for SiC power MOSFET Model. *J Integr Circuits Syst*, 18. https://doi.org/10.29292/jics.v18i2.756
34. Pan Z, Liu Y, Ren D, et al. (2023) A MOSFET EMC modeling method based on electrical characteristic measurement and simplex optimization and particle swarm optimization. *Int J Circ Theor Appl* 6: 2936–2955. https://doi.org/10.1002/cta.3856
35. Borghese A, Riccio M, Maresca L, et al. (2023) A scalable SPICE electrothermal compact model for SiC MOSFETs: A comparative study between the LEVEL-3 and the BSIM. *Key Eng Mater* 947. https://doi.org/10.4028/p-hmxz8o
36. Cusumano A, Crimi D, Raffa A, et al. (2023) SPICE-based model validation for 1200 V AcepackTM Drive traction power module. *International Symposium on Electromagnetic Compatibility—EMC Europe*, Krakow, Poland. https://doi.org/10.1109/EMCEurope57790.2023.10274154
37. Bottaro E, Rizzo S (2023) An overview of strengths and weaknesses in using MOSFET experience for modeling GaN HEMT. *Energies* 16: 6574. https://doi.org/10.3390/en16186574

AIMS Press